Free-Space Optical Communication with Nonzero Boresight Pointing Errors

Fan Yang, Julian Cheng, *Senior Member, IEEE,* and Theodoros A. Tsiftsis, *Senior Member, IEEE*

***Abstract*—The performance of free-space optical (FSO) communication systems is compromised by atmospheric fading and pointing errors. The pointing errors are widely considered as a combination of two components: boresight and jitter. A statistical model is investigated for pointing errors with nonzero boresight by taking into account the laser beamwidth, detector aperture size, and jitter variance. A novel closed-form probability density function (PDF) is derived for this new nonzero boresight pointing error model. Furthermore, we obtain closed-form PDF for the composite lognormal turbulence channels and finite series approximate PDF for the composite Gamma-Gamma turbulence channels, which is suitable for terrestrial FSO applications impaired by building sway. We conduct error rate analysis of on-off keying signaling with intensity modulation and direct detection over the lognormal and Gamma-Gamma fading channels. Asymptotic error rate analysis and outage probability of such a system are also presented based on the derived composite PDFs. It is shown that the boresight can only affect the coding gain, while the diversity order is determined by the atmospheric fading effect as well as the pointing error effect.**

I. Introduction

In free-space optical (FSO) communication systems, laser beams are transmitted through atmosphere, ranging from hundreds of meters to several kilometers in terrestrial solutions and to thousands of kilometers in earth-to-satellite links [1]. Such systems are vulnerable to both atmospheric attenuation and pointing errors, which can severely deteriorate its error rate performance.

In terrestrial FSO communication systems, the transceivers are often positioned at the top of tall buildings to obtain a line of sight. In such systems, the atmospheric turbulence, building sway, building vibration and thermal expansion of building can degrade the link performance. The atmospheric turbulence can cause random temporal and spatial irradiance fluctuation in the optical beam. The building sway, building vibration and thermal expansion of building can result in pointing errors that consist of two components: boresight and jitter. The boresight is the fixed displacement between beam center and center of the detector. Although typical terrestrial FSO systems are initially installed with near zero boresight error, the boresight is still considerable due to the thermal expansion of the building. In [2], the pointing errors are recorded over three days in a $TerraLink$ laser communication system. The radial displacement shows a cyclical pattern every 24 hours, which suggests the thermal expansion of the building plays an important role in pointing errors. The reported boresight can be as high as 0.3mrad [2]. In [3], the values of boresight in the range of $0.0039 - 0.0117\text{mrad}$ are used. In [4], the author considers boresight up to 0.03mrad in a horizontal FSO link. The jitter is the random offset of the beam center at detector plane, which is mainly caused by building sway and building vibration. The typical value of jitter standard deviation in a terrestrial FSO system is below 0.3mrad [2]. In [3], the jitter standard deviations of $0.0033 - 0.0100\text{mrad}$ are used. In [4], the author considers jitter standard deviation up to 0.01mrad.

In satellite-to-ground and intersatellite communications, the transmitter and receiver have high relative velocity, and there is mechanical noise due to satellite-based motion and gimbal friction [5]. Thus, it is difficult to realize perfect tracking, while jitter and boresight can also arise as residual pointing error.

Numerous studies on pointing error effects have been reported. In [6], the author proposes a mathematical model to minimize the transmitter power and the beam divergence angle in an urban optical wireless communication system with pointing errors caused by building sway. In [7], a maximum-likelihood estimator is developed to estimate the boresight and jitter component of the pointing error. In this system model, a point detector and nonzero boresight component are assumed. In a follow-up work [4], the same authors further consider the effects of atmospheric turbulence for lognormal and Gamma-Gamma fading channels, and they adopt a wave-optics based approach to evaluate the channel capacity. In [8], a statistical pointing error model is proposed by considering the laser beamwidth, jitter variance, and detector size. In this model, a closed-form probability density function (PDF) of the pointing error loss factor is derived by assuming that the pointing error has zero boresight. In [8], the size of detector area is taken into consideration. When the size of the detector area becomes negligibly small, this pointing error loss factor coincides with the one derived for the point detector in earlier works [6], [9]. Furthermore, the authors derive the optimal beamwidth to maximize the channel capacity at a given probability of outage. In [10], the error rate performance of FSO links over K-distributed turbulence channels in the presence of pointing error is studied by assuming intensity modulation direct detection (IM/DD) with on-off keying (OOK). The system under study uses the same pointing error model developed in [8]. The average bit-error rate (BER) is presented in closed-form using the Meijer G-function. In a related work [11], the authors study the BER performance of a heterodyne differential phase shift keying optical wireless communication system in the presence of pointing error over the Gamma-

F. Yang and J. Cheng are with the School of Engineering, The University of British Columbia, Kelowna, BC, Canada. (e-mail: {fan.yang, julian.cheng}@ubc.ca)

T. A. Tsiftsis is with the Department of Electrical Engineering, Technological Educational Institute of Lamia, Lamia, Greece. (e-mail: tsiftsis@teilam.gr)

Gamma turbulence channels. In [12], two optimization models are proposed to mitigate the pointing error effects with zero boresight by taking into account the transmitter power, wavelength, transmitter and receiver telescope gains. In [13], M-ary pulse-position modulation is investigated with impairments from atmospheric turbulence and pointing error with zero boresight. In [14], asymptotic BER performance is analyzed for FSO communication systems using transmit laser selection over atmospheric turbulence channels with the same pointing error model developed in [8]. A statistical channel model is recently proposed for multiple-input multiple-output (MIMO) FSO communication systems over atmospheric fading channels with pointing errors [15]. Both outage probability and diversity order are studied, and it is found that the diversity order is determined by pointing error effects other than the number of transmitters or receivers. More recently, the pointing error model in [8] is generalized by modeling the radial displacement distance with a Hoyt or Nakagami-q distribution [16], which allows the horizontal and elevation jitters to have nonidentical jitter standard deviations.

The pointing error model developed in [8] is widely used in the literature [10], [11], [13], [14]. In this model, the boresight component of pointing error is assumed to be zero, and both horizontal and elevation displacements are assumed to follow an independent, identically distributed zero-mean Gaussian distribution [9]. As a result, the random radial displacement at the receiver is Rayleigh distributed. In our work, we assume nonzero boresight component and assess the performance of terrestrial FSO systems. We derive a statistical model to describe the pointing error effects with nonzero boresight components by considering a finite size circular detector. We obtain a novel closed-form PDF of our generalized pointing error model. Our pointing error PDF specializes to the one in [8] when the boresight error is zero. Furthermore, we derive a closed-form PDF for the composite lognormal channels and an approximate series PDF for the composite Gamma-Gamma channels using our new pointing error model. Our series PDF for the composite Gamma-Gamma channels is applicable when $\gamma^2 > \alpha$, where γ is the ratio between the equivalent beamwidth and jitter standard deviation, and α is a parameter related to the large scale turbulence cells in Gamma-Gamma turbulence fading model. We find that the condition $\gamma^2 > \alpha$ is satisfied in many terrestrial FSO systems impaired by building sway. Finally, we study both the error rate performance, asymptotic error rate performance, and outage probability for an OOK IM/DD based FSO system in the presence of nonzero boresight pointing errors.

The remainder of this paper is organized as follows. Section II describes our system model and derives the closed-form PDF of our pointing error model. We review two important atmospheric turbulence channels and derive closed-form PDF for the composite lognormal channels and series PDF for composite Gamma-Gamma turbulence channels when $\gamma^2 > \alpha$. We present several examples where $\gamma^2 > \alpha$ is satisfied and show that $\gamma^2 > \alpha$ is valid in many terrestrial FSO systems impaired by building sway. In Section III, we derive expressions of BER, asymptotic BER, and outage probability of an FSO system over the lognormal and Gamma-Gamma turbulence channels with nonzero boresight pointing errors. Section IV presents some numerical results, and Section V makes several important conclusions.

II. Turbulence Channels with Nonzero Boresight Pointing Errors

OOK modulation is widely used in practical FSO systems [24], [25] since optical communication systems with higher order modulation are complex to implement. In this work, we consider an OOK FSO system with IM/DD. The transmitter modulates the data bits directly onto the intensity of an optical beam, which propagates through an atmospheric turbulence channel in the presence of pointing errors. Since the channel coherence time is on the order of msec and the data rate is assumed to be on the order of Gbps, we can therefore adopt a slow fading channel model. The received optical power is converted into an electrical signal through direct detection at the photodetector. Assuming additive white Gaussian noise (AWGN) for the thermal/shot noise and unit detector responsitivity, we can express the received signal y at the detector as

$$y = hx + n \tag{1}$$

where x is the transmit intensity being either 0 or $2P_t$, where P_t is the average transmitted optical power, h is the channel gain, n is zero-mean AWGN with variance σ_n^2. Following [8], [11], [15], we assume that the off-axis scintillation changes slowly near the spot of boresight displacement, and use a constant value of scintillation index to characterize the atmospheric turbulence. Therefore, the pointing error and atmospheric fading are independent, and the channel gain h can be expressed as $h = h_l h_p h_a$, where h_l represents the path loss which is a constant at given weather condition and link distance, h_p is the pointing error loss factor, and h_a is the atmospheric fading loss factor. Note that pointing error loss factor h_p and atmospheric fading loss factor h_a are both random variables (RVs).

A. Nonzero Boresight Pointing Error Model

When a Gaussian beam propagates through distance z from the transmitter to a circular detector with aperture radius a, and the instantaneous radial displacement between the beam centroid and the detector center is r, the fraction of the collected power at receiver can be approximated as [8]

$$h_p(r; z) \approx A_0 \exp\left(-\frac{2r^2}{w_{z_{eq}}^2}\right) \tag{2}$$

where A_0 is the fraction of the collected power at $r = 0$, and $w_{z_{eq}}$ is the equivalent beamwidth. We have $A_0 = [\mathrm{erf}(v)]^2$ and $w_{z_{eq}}^2 = w_z^2 \frac{\sqrt{\pi}\mathrm{erf}(v)}{2v\exp(-v^2)}$, where $v = \sqrt{\pi/2}\frac{a}{\omega_z}$ is the ratio between aperture radius and beamwidth, and $\mathrm{erf}(x) = \frac{2}{\sqrt{\pi}}\int_0^x e^{-t^2}dt$ is the error function. The beamwidth w_z can be approximated by $w_z = \theta z$, where θ is the transmit divergence angle describing the increase in beam radius with distance from the transmitter. For example, at a range of 1 km, a 1 mrad divergence produces a beam radius of 1m at receiver.

The approximation in (2) is accurate when $w_z/a > 6$, which is satisfied in typical terrestrial FSO communication systems.

At the receiver aperture plane, we can express the radial displacement vector as $\mathbf{r} = [r_x, r_y]^T$, where r_x and r_y, respectively, denote the displacements located along the horizontal and elevation axes at the detector plane. We consider a nonzero boresight error in addition to the random jitters, and model r_x and r_y as nonzero mean Gaussian distributed RVs, i.e., $r_x \sim \mathcal{N}(\mu_x, \sigma_x^2)$, $r_y \sim \mathcal{N}(\mu_y, \sigma_y^2)$. Then the radial displacement $r = |\mathbf{r}| = \sqrt{r_x^2 + r_y^2}$ follows the Beckmann distribution [26]

$$f_r(r) = \frac{r}{2\pi\sigma_x\sigma_y} \times \int_0^{2\pi} \exp\left(-\frac{(r\cos\phi - \mu_x)^2}{2\sigma_x^2} - \frac{(r\sin\phi - \mu_y)^2}{2\sigma_y^2}\right) d\phi. \tag{3}$$

The Beckmann distribution is also known as lognormal-Rician distribution [27], [28], which is used to describe the PDF of fading channels in general. It is a versatile model which applies to a variety of distributions. For examples, it can specialize to Rayleigh when $\mu_x = \mu_y = 0, \sigma_x = \sigma_y$; Rician with $\mu_x^2 + \mu_y^2 \neq 0, \sigma_x = \sigma_y$; Hoyt distribution when $\mu_x = \mu_y = 0, \sigma_x \neq \sigma_y$ [16]; and single-sided Gaussian when $\mu_x = \mu_y = \sigma_x = 0, \sigma_y \neq 0$ [29].

In satellite FSO communication systems, it is widely accepted that the jitter variance is the same for both horizontal and elevation axes [21], [22]. In terrestrial FSO systems, however, the jitter is mainly caused by turbulence and building motion. Since the turbulence cells randomly appear on the beam path, and the building might be considered to sway in orthogonal and parallel directions to the beam path with equal probabilities, we can therefore assume $\sigma_x^2 = \sigma_y^2 = \sigma_s^2$ [8], [11], [15]. As a result, the PDF of radial displacement r in (3) becomes Rician

$$f_r(r) = \frac{r}{\sigma_s^2} \exp\left(\frac{-(r^2 + s^2)}{2\sigma_s^2}\right) I_0\left(\frac{rs}{\sigma_s^2}\right) \tag{4}$$

where $s = \sqrt{\mu_x^2 + \mu_y^2}$ is the boresight displacement, and $I_0(\cdot)$ is the modified Bessel function of the first kind with order zero. From (2) and (4), we derive the PDF of nonzero boresight pointing error as

$$f_{h_p}(h_p) = \frac{\gamma^2 \exp\left(\frac{-s^2}{2\sigma_s^2}\right)}{A_0^{\gamma^2}} h_p^{\gamma^2 - 1} I_0\left(\frac{s}{\sigma_s^2}\sqrt{\frac{-w_{z_{eq}}^2 \ln\frac{h_p}{A_0}}{2}}\right), \quad 0 \leq h_p \leq A_0 \tag{5}$$

where $\gamma = w_{z_{eq}}/2\sigma_s$ is the ratio between the equivalent beamwidth and jitter standard deviation, which is a measure of the severity of the pointing error effect. If we consider zero boresight error with $s = 0$, our pointing error model in (5) specializes to the one in [8]. Our analytical result in (5) is accurate when $w_z/a > 6$. In Appendix A, we compare our derived PDF of h_p in (5) with the exact PDF, which is obtained numerically, without using (2) to show the accuracy of our analytical model. In Appendix B, we derive the moments of h_p as

$$E\left[h_p^n\right] = \frac{A_0^n \gamma^2}{n + \gamma^2} \exp\left(-\frac{ns^2}{(n + \gamma^2)2\sigma_s^2}\right) \tag{6}$$

where $E[\cdot]$ denotes the expectation.

B. Atmospheric Fading Channels

In order to study the effects of turbulence-induced fading on the performance of FSO systems, several statistical models characterizing atmospheric fading have been proposed. For weak turbulence conditions, we use the lognormal fading model to characterize the atmospheric fading h_a whose PDF is given by

$$f_{h_a}(h_a) = \frac{1}{2h_a\sqrt{2\pi\sigma_X^2}} \exp\left(-\frac{(\ln h_a + 2\sigma_X^2)^2}{8\sigma_X^2}\right) \tag{7}$$

where σ_X^2 is the log-amplitude variance given by $\sigma_X^2 \approx \sigma_R^2/4 = 0.31k^{7/6}C_n^2 z^{11/6}$ [8], where σ_R^2 is the Rytov variance for a plane wave, C_n^2 is the index of refraction structure parameter of atmosphere, and $k = 2\pi/\lambda$ is the optical wavenumber with λ being the wavelength. The parameters of the lognormal fading model can be measured directly for FSO systems [30]. For medium to strong turbulence conditions, we use the Gamma-Gamma turbulence model to characterize the atmospheric fading h_a whose PDF is given by

$$f_{h_a}(h_a) = \frac{2(\alpha\beta)^{(\alpha+\beta)/2}}{\Gamma(\alpha)\Gamma(\beta)} h_a^{\frac{\alpha+\beta}{2}-1} K_{\alpha-\beta}\left(2\sqrt{\alpha\beta h_a}\right) \tag{8}$$

where $\Gamma(\cdot)$ is the Gamma function, and $K_{\alpha-\beta}(\cdot)$ is the modified Bessel function of the second kind of order $\alpha - \beta$. The parameters α and β are related to the small scale and large scale eddies respectively.

Depending on the value of the Rytov variance, we can approximately categorize the turbulence regime as follows [32]: the weak turbulence regime ($\sigma_R^2 < 0.3$) and the moderate to strong turbulence regime ($\sigma_R^2 \geq 0.3$).

C. Composite PDF with Generalized Pointing Error

The PDF of channel gain $h = h_l h_p h_a$ can be calculated as [8]

$$\begin{aligned} f_h(h) &= \int f_{h|h_a}(h|h_a) f_{h_a}(h_a) dh_a \\ &= \int \frac{1}{h_a h_l} f_{h_p}\left(\frac{h}{h_a h_l}\right) f_{h_a}(h_a) dh_a. \end{aligned} \tag{9}$$

In weak turbulence conditions, we use lognormal fading model to characterize the atmospheric turbulence fading. We substitute (7) into (9), and after some mathematical manipulation, the composite PDF of lognormal fading with the pointing error model in (5) can be obtained as

$$f_{LN}(h) = \frac{\gamma^2 \exp(u_a)}{2(A_0 h_l)^{\gamma^2}} h^{\gamma^2 - 1} \mathrm{erfc}\left(\frac{\ln\frac{h}{A_0 h_l} + u_b}{u_c}\right) \tag{10}$$

where $u_a = \frac{s^2}{\sigma_s^2} + 2\sigma_X^2\gamma^2 + 2\sigma_X^2\gamma^4$, $u_b = \frac{6s^2}{\omega_{z_{eq}}^2} + 2\sigma_X^2 + 4\sigma_X^2\gamma^2$, $u_c = \sqrt{8\left(\frac{4s^2\sigma_s^2}{\omega_{z_{eq}}^4} + \sigma_X^2\right)}$, and $\mathrm{erfc(u)} = 1 - \mathrm{erf(u)}$ is the complementary error function. It is worthy to note that our PDF in (10) can specialize to eq. (14) in [8] when we set the boresight to zero ($s = 0$).

Since h_l is a constant, while h_p and h_a are independent RVs, The nth moment of h can be obtained as $E[h^n] = h_l^n E[h_p^n]E[h_a^n]$. With the derived moments for h_p in (6) and the moments of the lognormal RV, we have

$$E[h^n] = \frac{(A_0 h_l)^n \gamma^2}{n+\gamma^2} \times \exp\left(-2\sigma_X^2 n + 2\sigma_X^2 n^2 - \frac{ns^2}{(n+\gamma^2)2\sigma_s^2}\right). \tag{11}$$

For medium to strong turbulence conditions, we model h_a as a Gamma-Gamma distributed RV. After some mathematical derivation shown in Appendix C, we obtain a finite series approximation of the composite PDF as

$$f_{GG}(h) \approx \widetilde{f}_{GG}(h) = \sum_{j=0}^{J}\left\{\frac{1}{j!}\left(\frac{\alpha\beta}{A_0 h_l}\right)^j \left(v_j(\alpha,\beta)h^{\beta-1+j} - v_j(\beta,\alpha)h^{\alpha-1+j}\right)\right\} \tag{12a}$$

where

$$v_j(\alpha,\beta) = \frac{\gamma^2\pi\left(\frac{\alpha\beta}{A_0 h_l}\right)^\beta \exp\left(-\frac{s^2}{2\sigma_s^2} - \frac{s^2\gamma^2/\sigma_s^2}{2\beta-2\gamma^2+2j}\right)\sin^{-1}((\alpha-\beta)\pi)}{\Gamma(\alpha)\Gamma(\beta)\Gamma(j-(\alpha-\beta)+1)| - (\beta-\gamma^2+j)|} \tag{12b}$$

and $J = \lfloor \gamma^2 - \alpha \rfloor$. Therefore (12a) is an approximation[1] of the composite PDF of Gamma-Gamma fading with pointing error. Our composite PDF in (12a) is applicable under the condition $\gamma^2 > \alpha$. Using a rough approximation, we can show that the condition $\gamma^2 > \alpha$ corresponds to $\frac{w_z^2}{4\sigma_s^2} > \max\{6, 2.31\sigma_R^{4/5}\}$. Now we present some examples where this condition holds: When $\sigma_R^2 = 5.0$ and the jitter angle is $0.3\mathrm{mrad}$, the transmit divergence is larger than $1.28\mathrm{mrad}$. When $\sigma_R^2 = 25.0$ and the transmit beam divergence is $2\mathrm{mrad}$, the jitter angle is less than $0.35\mathrm{mrad}$. In terrestrial FSO systems with link distance less than $5\mathrm{km}$, the system parameters have the following typical values: $5 \sim 20\mathrm{cm}$ for the receiver diameter, $2 \sim 10\mathrm{mrad}$ for the transmit divergence, and $0 \sim 0.3\mathrm{mrad}$ for the boresight and jitter angle [2], [17]. It can be shown that such systems generally operate under the condition $\gamma^2 > \alpha$. However, in applications with long link range or narrow beam divergence, our PDF in (12a) is not applicable since $\gamma^2 > \alpha$ may not hold in such applications. In the rest of paper, we assume $\gamma^2 > \alpha$ unless otherwise stated. In (12a), the parameters α, β are required to satisfy $(\alpha - \beta) \notin \mathbb{Z}$. When $(\alpha - \beta) \in \mathbb{Z}$, one can add a small value ε to α to satisfy the condition $(\alpha - \beta) \notin \mathbb{Z}$ [33]. The value of ε is empirically chosen, which should be small (i.e. 10^{-3}) that will not change the Gamma-Gamma distribution dramatically. For example, if we have $\alpha = 2.12, \beta = 1.12$, we can add 0.001 to α, and use $\alpha = 2.121$ in the Gamma-Gamma model.

[1]This finite series approximation is accurate for strong turbulence conditions, but it can be inaccurate for weak turbulence conditions. A large boresight and jitter can also make the series inaccurate.

Similar to the moments obtained for composite lognormal channel, using (6) and the moments for the Gamma-Gamma RV we can obtain the nth moment of h as

$$E[h^n] = \frac{(A_0 h_l)^n \gamma^2 \Gamma(\alpha+n)\Gamma(\beta+n)}{(n+\gamma^2)\Gamma(\alpha)\Gamma(\beta)(\alpha\beta)^n} \exp\left(-\frac{ns^2}{(n+\gamma^2)2\sigma_s^2}\right). \tag{13}$$

III. Error Rate Performance

Following the system model described in Section II, the BER of IM/DD with OOK modulation conditioned on the channel gain is

$$P_e(e|h) = Q\left(\frac{P_t h}{\sigma_n}\right) = \frac{1}{2}\mathrm{erfc}\left(\frac{P_t h}{\sqrt{2}\sigma_n}\right) \tag{14}$$

where $Q(x) = \frac{1}{\sqrt{2\pi}}\int_x^\infty \exp\left(-\frac{u^2}{2}\right)du$ is the Gaussian Q-function. The average BER can be obtained as

$$P_e = \int_0^\infty P_e(e|h) f_h(h) dh. \tag{15}$$

According to (1), we have $E[x^2] = 2P_t^2$. Assuming a slow fading channel, the instantaneous signal-to-noise ratio (SNR) is defined as $\mathrm{SNR} = \frac{2P_t^2 h^2}{\sigma_n^2}$. We define the average SNR as the received SNR when there is no fading and pointing error ($E[h^2] = 1$). Thus, we have the average SNR as $\overline{\mathrm{SNR}} = \frac{2P_t^2}{\sigma_n^2}$.

A. Bit-Error Rate

1) Composite lognormal model: We derive the average BER of lognormal fading with nonzero boresight pointing error by substituting (10) into (15). The BER expression can be written as

$$P_{e,LN} = \frac{\gamma^2 \exp(u_a)}{4(A_0 h_l)^{\gamma^2}} \times \int_0^\infty h^{\gamma^2-1}\mathrm{erfc}\left(\frac{\ln\frac{h}{A_0 h_l} + u_b}{u_c}\right)\mathrm{erfc}\left(\frac{P_t}{\sqrt{2}\sigma_n}h\right)dh. \tag{16}$$

Using a change of variable rule, eq. (16) can be expressed as

$$P_{e,LN} = \frac{\gamma^2 u_c}{4}\exp\left(u_a - \gamma^2 u_b\right) \times \int_{-\infty}^\infty \exp(\gamma^2 u_c x)\mathrm{erfc}(x)\mathrm{erfc}\left(\frac{P_t A_0 h_l}{\sqrt{2}\sigma_n \exp(u_b - u_c x)}\right)dx. \tag{17}$$

By introducing an auxiliary parameter B and partitioning the integration interval in (17) into $[-\infty, B]$ and $[B, \infty]$, we can

$$P_{e,LN} = \frac{\gamma^2 u_c}{4} \exp\left(u_a - \gamma^2 u_b\right) \times \int_{-\infty}^{B} \exp\left(\gamma^2 u_c x\right) \mathrm{erfc}\left(x\right) \mathrm{erfc}\left(\frac{P_t A_0 h_l}{\sqrt{2}\sigma_n} \exp\left(u_c x - b\right)\right) dx + R_B \tag{18}$$

rewrite (17) as (18), where R_B is the approximation error given by

$$R_B = \frac{\gamma^2 u_c}{4} \exp\left(u_a - \gamma^2 u_b\right) \times \int_{B}^{\infty} \exp(\gamma^2 u_c x) \mathrm{erfc}(x) \mathrm{erfc}\left(\frac{P_t A_0 h_l}{\sqrt{2}\sigma_n \exp(u_b - u_c x)}\right) dx. \tag{19}$$

In Appendix D, it is shown that the approximation error R_B can be upper bounded by

$$R_B < \frac{\sqrt{\pi}\gamma^2 u_c}{8} \exp\left(u_a - \gamma^2 u_b + \frac{\gamma^4 u_c^2}{4}\right) \mathrm{erfc}\left(B - \frac{\gamma^2 u_c}{2}\right). \tag{20}$$

We quantify R_B under various system parameters and calculate the values of B for different R_B. The results are presented in Appendix D, showing that the approximation error R_B decreases rapidly with increasing B. We can always adjust the value of B to make R_B arbitrarily small. Therefore, eq. (18) can be accurately approximated as

$$P_{e,LN} \approx \widetilde{P}_{e,LN} = \frac{\gamma^2 u_c}{4} \exp\left(u_a - \gamma^2 u_b\right) \times \int_{-\infty}^{B} \exp(\gamma^2 u_c x) \mathrm{erfc}(x) \mathrm{erfc}\left(\frac{P_t A_0 h_l}{\sqrt{2}\sigma_n \exp(u_b - u_c x)}\right) dx. \tag{21}$$

Using a series expansion of the complementary error function [34, eq. (06.27.06.0002.01)]

$$\mathrm{erfc}(z) = 1 - \frac{2}{\sqrt{\pi}} \sum_{k=0}^{\infty} \frac{(-1)^k z^{2k+1}}{k!(2k+1)} \tag{22}$$

and an integral identity [34, eq. (06.27.21.0011.01)]

$$\int e^{bz} \mathrm{erfc}(az) dz = \frac{1}{b}\left(e^{bz}\mathrm{erfc}(az) - e^{\frac{b^2}{4a^2}} \mathrm{erf}\left(\frac{b}{2a} - az\right)\right) \tag{23}$$

we derive an infinite series expression of the BER in (21) as (24) at the top of next page, where

$$S_j = \exp((\gamma^2 + 2j + 1)u_c B)\mathrm{erfc}(B) + \exp\left((\gamma^2 + 2j + 1)^2 u_c^2/4\right)\mathrm{erfc}((\gamma^2 + 2j + 1)u_c/2 - B). \tag{25}$$

The infinite series in (24) can be rigorously shown to be convergent, and a detailed proof is presented in Appendix E.

2) Composite Gamma-Gamma Model: For the Gamma-Gamma fading with nonzero boresight pointing error, we substitute (12a) into (15) to find its BER. Using an integral formula [34, eq. (06.27.21.0132.01)]

$$\int_0^{\infty} t^{\alpha-1} \mathrm{erfc}(t) = \frac{1}{\sqrt{\pi}\alpha} \Gamma\left(\frac{\alpha+1}{2}\right) \tag{26}$$

we can obtain the approximate BER in terms of a finite series as (27). We comment (27) is obtained without additional approximations over those in (12a). The approximation error defined as $\varepsilon(P_e) = |P_e - \widetilde{P}_e|$ is discussed in Appendix F. When P_t is beyond the minimum required value in Table IV, we can guarantee the relative error $\frac{\varepsilon(P_{e,GG})}{P_{e,GG}}$ and $\frac{\varepsilon(P_{out,GG})}{P_{out,GG}}$ less than 10^{-6}, where $P_{out,GG}$ denotes the outage probability of system in the composite Gamma-Gamma fading case and $\varepsilon(P_{out,GG})$ denotes the approximation error $|P_{out,GG} - \widetilde{P}_{out,GG}|$. With the setting $s/a = 1.0$ and $\sigma_s/a = 1.0$, the minimum required P_t is below -10 dBm, which can be satisfied for practical FSO systems.

B. Asymptotic Error Rate Analysis

At asymptotically high SNR, average symbol error probability of an uncoded system in fading channels can be accurately approximated as $P_e^{\infty} = (G_c \cdot \overline{\mathrm{SNR}})^{-G_d}$, where G_d is the diversity order indicating how fast the BER decreases with $\overline{\mathrm{SNR}}$ in high SNR region, and G_c is the coding gain determining the shift of the BER curve in $\overline{\mathrm{SNR}}$ relative to the benchmark curve $(\overline{\mathrm{SNR}})^{-G_d}$. The asymptotic BER P_e^{∞} can reveal the behavior of BER in high SNR region, which is helpful in conceptual understanding of performance limiting factors in communications over fading channels [36]. The diversity order and coding gain are determined from instantaneous SNR's PDF through its behavior near the origin. The PDF of channel gain can be expanded into power series as [36]

$$\lim_{h \to 0} f_h(h) = a h^t + g_t(h) \tag{28}$$

where $g_t(h)$ satisfies $\lim_{h\to 0} \frac{g_t(h)}{h^t} = 0$. Considering $\mathrm{SNR} = \frac{2P_t^2(h)^2}{\sigma_n^2}$, the diversity order and coding gain are obtained as [36]

$$G_d = \frac{t+1}{2} \tag{29}$$

and

$$G_c = \left(\frac{2^{\frac{t-3}{2}} a \Gamma\left(\frac{t}{2}+1\right)}{\sqrt{\pi}\left(\frac{t+1}{2}\right)}\right)^{-\frac{2}{t+1}}. \tag{30}$$

In the following, we first derive the power series expansion of the PDF near its origin, then we obtain the diversity order and coding gain from (29) and (30). The asymptotic BER is obtained from $P_e^{\infty} = (G_c \cdot \overline{\mathrm{SNR}})^{-G_d}$. For the composite lognormal fading with pointing error, we obtain the PDF of the channel gain h near the origin by applying the limit operation to (10) directly, the result is shown as

$$\lim_{h\to 0} f_{LN}(h) = \frac{\gamma^2}{(A_0 h_l)^{\gamma^2}} \exp\left(u_a\right) h^{\gamma^2 - 1} + g_{\gamma^2 - 1}(h). \tag{31}$$

$$\widetilde{P}_{e,LN} = \frac{\gamma^2 u_c}{4}\exp\left(u_a-\gamma^2 u_b\right)\left\{\frac{1}{\gamma^2 u_c}\left[\exp(\gamma^2 u_c B)\mathrm{erfc}(B)+\exp\left(\frac{\gamma^4 u_c^2}{4}\right)\mathrm{erfc}\left(\frac{\gamma^2 u_c}{2}-B\right)\right]\right.$$
$$\left.-\frac{2}{\sqrt{\pi}}\sum_{j=0}^{\infty}\left[\frac{(-1)^j}{j!(2j+1)}\left(\frac{P_t}{\sqrt{2}\sigma_n}A_0 h_l\right)^{2j+1}\frac{\exp(-u_b(2j+1))}{(2j+1+\gamma^2)u_c}S_j\right]\right\} \tag{24}$$

$$P_{e,GG}\approx\widetilde{P}_{e,GG}=\frac{1}{2\sqrt{\pi}}\sum_{j=0}^{J}\left\{\frac{1}{j!}\left(\frac{2\alpha\beta}{A_0 h_l}\right)^j\left(\frac{2^\beta\Gamma\left(\frac{\beta+j+1}{2}\right)}{\beta+j}v_j(\alpha,\beta)\left(\frac{2P_t^2}{\sigma_n^2}\right)^{-\frac{\beta+j}{2}}\right.\right.$$
$$\left.\left.-\frac{2^\alpha\Gamma\left(\frac{\alpha+j+1}{2}\right)}{\alpha+j}v_j(\beta,\alpha)\left(\frac{2P_t^2}{\sigma_n^2}\right)^{-\frac{\alpha+j}{2}}\right)\right\} \tag{27}$$

From (31), we obtain the diversity order as $G_d=\frac{\gamma^2}{2}=\frac{w_{z_{eq}}^2}{8\sigma_s^2}$. This indicates that the diversity order is determined by the ratio between equivalent beamwidth and jitter standard deviation. More specifically, the boresight component of pointing error does not affect the diversity order in lognormal fading channel. The coding gain can also be obtained from (31) as

$$G_c=\left[\frac{2^{\gamma^2-1}\Gamma\left(\frac{\gamma^2}{2}+\frac{1}{2}\right)\exp\left(u_a\right)}{\sqrt{\pi}(A_0 h_l)^{\gamma^2}}\right]^{-\frac{2}{\gamma^2}}. \tag{32}$$

With $\overline{\mathrm{SNR}}=\frac{2P_t^2}{\sigma_n^2}$, we can present the asymptotic bit-error rate as

$$P_{e,LN}^{\infty}=\frac{2^{\gamma^2-1}\Gamma\left(\frac{\gamma^2}{2}+\frac{1}{2}\right)\exp\left(u_a\right)}{\sqrt{\pi}(A_0 h_l)^{\gamma^2}}\left(\frac{2P_t^2}{\sigma_n^2}\right)^{-\frac{\gamma^2}{2}}. \tag{33}$$

For the Gamma-Gamma composite fading channels, we derive the power series expansion of PDF near the origin in Appendix C, and it is given by

$$\lim_{h\to 0}f_{GG}(h)=v_0(\alpha,\beta)h^{\beta-1}+g_{\beta-1}(h) \tag{34}$$

where $v_0(\alpha,\beta)$ follows the definition in (12b) and we have assumed $\gamma^2>\alpha$. From (34), we obtain the diversity order as $G_d=\beta/2$ and the coding gain as

$$G_c=\left[\frac{2^{\beta-1}\Gamma\left(\frac{\beta}{2}+\frac{1}{2}\right)\exp\left(-\frac{s^2}{2\sigma_s^2}+\frac{-s^2\gamma^2/\sigma_s^2}{2\beta-2\gamma^2}\right)\left(\frac{\alpha\beta}{A_0 h_l}\right)^\beta}{\Gamma(\alpha)\Gamma(\beta)\sin((\alpha-\beta)\pi)\Gamma(-(\alpha-\beta)+1)|\gamma^2-\beta|\beta}\right.$$
$$\left.\times\Gamma\left(\frac{\beta+1}{2}\right)\sqrt{\pi}\gamma^2\right]^{-\frac{2}{\beta}}. \tag{35}$$

Thus, the asymptotic bit-error rate can be expressed as

$$P_{e,GG}^{\infty}=\frac{2^{\beta-1}\Gamma\left(\frac{\beta}{2}+\frac{1}{2}\right)\exp\left(-\frac{s^2}{2\sigma_s^2}+\frac{-s^2\gamma^2/\sigma_s^2}{2\beta-2\gamma^2}\right)\left(\frac{\alpha\beta}{A_0 h_l}\right)^\beta}{\Gamma(\alpha)\Gamma(\beta)\sin((\alpha-\beta)\pi)\Gamma(-(\alpha-\beta)+1)|\gamma^2-\beta|\beta}$$
$$\times\Gamma\left(\frac{\beta+1}{2}\right)\sqrt{\pi}\gamma^2\left(\frac{2P_t^2}{\sigma_n^2}\right)^{-\frac{\beta}{2}}. \tag{36}$$

Note that the diversity order is $G_d=\beta/2$ when $\gamma^2>\alpha$, which implies that the Gamma-Gamma fading effect is more dominant than the pointing error effect with respect to the BER performance at high average SNR region. However, when $\gamma^2<\alpha$, the diversity order will depend on both γ^2 and the boresight s. An explicit expression of diversity order for nonzero boresight pointing case is difficult to obtain. For the special case with zero boresight, the diversity order is given as $\min\{\gamma^2/2,\beta/2\}$ [37].

To evaluate the performance loss caused by boresight error, we define an SNR penalty factor in dB as

$$\mathrm{SNR}_{boresight}=10\log_{10}\left[\frac{\mathrm{SNR}_{P_e^\infty,\mathrm{nonzeroboresight}}}{\mathrm{SNR}_{P_e^\infty,\mathrm{zeroboresight}}}\right] \tag{37}$$

which represents the constant SNR loss caused by boresight error at certain error probability P_e^∞ when SNR is asymptotically large. From (33) and (36), we obtain the SNR penalty factor for the composite lognormal and the composite Gamma-Gamma fading, respectively, as

$$\mathrm{SNR}_{boresight,LN}=\frac{80}{\ln 10}\left[\frac{s}{\omega_{z_{eq}}}\right]^2 \tag{38}$$

and

$$\mathrm{SNR}_{boresight,GG}=\frac{40}{\ln 10}\left[\frac{s}{\sqrt{\omega_{z_{eq}}^2-4\sigma_s^2\beta}}\right]^2 \tag{39}$$

where we have assumed $\gamma^2>\alpha$, that is $w_{z_{eq}}^2>4\sigma_s^2\beta$ in (39). The results in (38) and (39) show that, for both composite lognormal and composite Gamma-Gamma cases, the boresight error imposes a constant SNR penalty on the error rate performance when SNR is large. As expected, larger beamwidth $\omega_{z_{eq}}$ can mitigate the adverse impact of the boresight error.

C. Outage Probability

In a slow fading FSO system with IM/DD OOK, we assume the receiver has perfect knowledge of channel gain, and the data rate of transmitter is R_0 bits/channel use. For

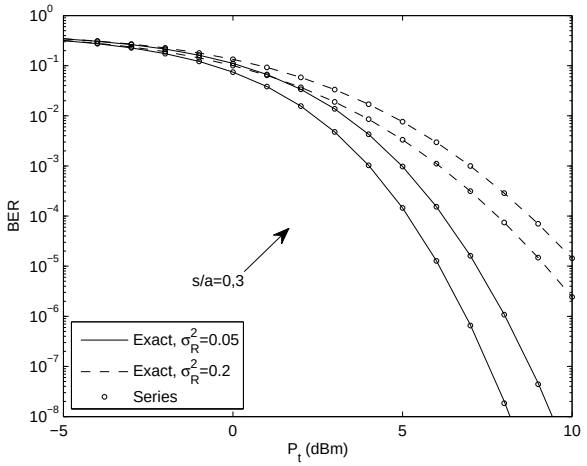

Fig. 1. BER performance of IM/DD OOK over the lognormal fading with zero and nonzero boresight pointing errors.

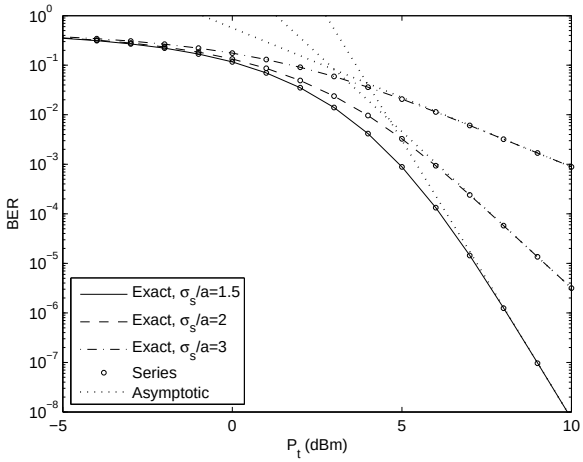

Fig. 2. BER for the composite lognormal channel ($\sigma_R^2 = 0.01, s/a = 2$) with different jitter values.

OOK signaling, the instantaneous capacity corresponding to a specific channel realization h' is given by [8]

$$\mathcal{C}(h') = \int \sum_x f_{y|x}(y|x) p_x(x) \log_2 \frac{f_{y|x}(y|x)}{f_y(y)} dy \qquad (40)$$

where $x \in \{0, 2P_t\}$, $p_x(x = 0) = p_x(x = 2P_t) = 0.5$, $f_{y|x}(y|x) = \frac{1}{\sqrt{2\pi\sigma_n^2}} \exp\left(\frac{(y-h'x)^2}{2\sigma_n^2}\right)$, $f_y(y) = \sum_x p_x(x) f_{y|x}(y|x)$. We define the outage probability as the probability that the instantaneous capacity $\mathcal{C}(h)$ is not sufficient to support the data rate R_0, and it is given by [8]

$$P_{out} = \text{Prob}(h < \mathcal{C}^{-1}(R_0)) \qquad (41)$$

which can be calculated as

$$P_{out} = \int_0^{h_0} f_h(h) dh \qquad (42)$$

where $h_0 = \mathcal{C}^{-1}(R_0)$. Therefore, we can use the composite PDF, which has been derived for different turbulence models, to calculate the outage probability at a given transmission rate. For weak turbulence condition, substituting (10) into (42) and using the integral identity in (23) we obtain the outage probability as (43) at the top of next page. For medium to strong turbulence conditions, by substituting (12a) into (42), we obtain the outage probability in (44).

It is worthy to mention that we can obtain the diversity order using the outage probability derived in (43) and (44), the derivation follows that in [15]. The results are $G_{d,LN} = \gamma^2/2$ and $G_{d,GG} = \beta/2$, which coincide with the ones obtained using the power series expansion approach.

IV. Numerical Results

In this section, we adopt the system settings shown in Table I, which are used in many practical terrestrial FSO communication systems [2], [17], [39]. Under two typical weather conditions shown in Table II [8], we carry out the error rate performance of an FSO communication system. In order to investigate the degradation effects induced by the

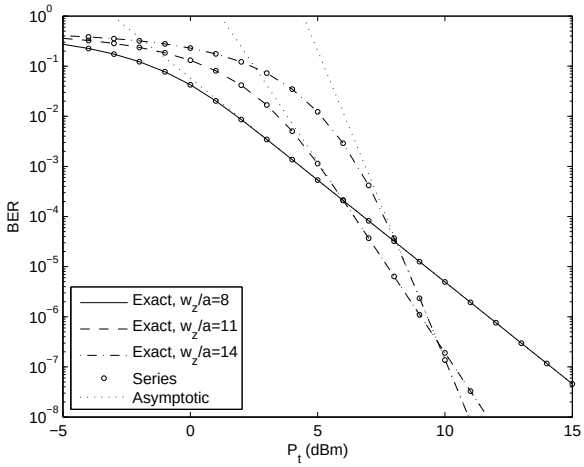

Fig. 3. BER for the composite lognormal channel ($\sigma_R^2 = 0.01, s/a = 2, \sigma_s/a = 1.5$) with different beamwidth values.

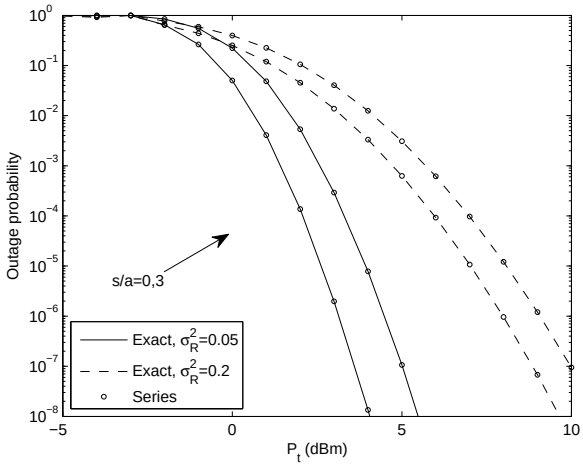

Fig. 4. Outage probability of an FSO system over the lognormal fading with zero and nonzero boresight pointing errors.

$$P_{out,LN} = \frac{1}{2}\left[\left(\frac{h_0}{A_0 h_l}\right)^{\gamma^2} \exp(u_a)\mathrm{erfc}\left(\frac{\ln\frac{h_0}{A_0 h_l} + u_b}{u_c}\right) + \exp\left(u_a - u_b\gamma^2 + \frac{u_c^2\gamma^4}{4}\right)\mathrm{erfc}\left(\frac{u_c\gamma^2}{2} - \frac{\ln\frac{h_0}{A_0 h_l} + u_b}{u_c}\right)\right] \tag{43}$$

$$P_{out,GG} \approx \widetilde{P}_{out,GG} = \frac{\exp\left(-\frac{s^2}{2\sigma_s^2}\right)\gamma^2\pi}{\Gamma(\alpha)\Gamma(\beta)\sin((\alpha-\beta)\pi)} \sum_{j=0}^{J}\left(\frac{\alpha\beta}{A_0 h_l}\right)^j \left(\frac{\left(\frac{\alpha\beta}{A_0 h_l}\right)^\beta \exp\left(\frac{-s^2\gamma^2/\sigma_s^2}{2\beta-2\gamma^2+2j}\right)}{\Gamma(j-(\alpha-\beta)+1)j!|-(\beta-\gamma^2+j)|(\beta+j)} h_0^{\beta+j} - \frac{\left(\frac{\alpha\beta}{A_0 h_l}\right)^\alpha \exp\left(\frac{-s^2\gamma^2/\sigma_s^2}{2\alpha-2\gamma^2+2j}\right)}{\Gamma(j+(\alpha-\beta)+1)j!|-(\alpha-\gamma^2+j)|(\alpha+j)} h_0^{\alpha+j}\right). \tag{44}$$

TABLE II
SAMPLE SYSTEM PARAMETERS UNDER LIGHT FOG AND CLEAR SKY WEATHER CONDITIONS

Weather	Visibility	Path loss (h_l)	C_n^2 level	Fading model	σ_R^2	Parameters
Light fog	0.5 km	0.008	$10^{-15}\mathrm{m}^{-2/3}$	Lognormal	0.05	$\sigma_X^2 = 0.0125$
					0.2	$\sigma_X^2 = 0.05$
Clear sky	10 km	0.9	$10^{-14}\mathrm{m}^{-2/3}$	Gamma-Gamma	0.6	$\alpha = 5.41, \beta = 3.78$
					2.0	$\alpha = 3.99, \beta = 1.70$

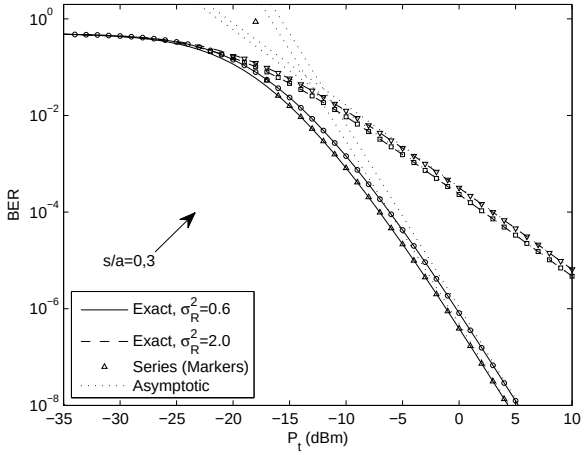

Fig. 5. BER performance of IM/DD OOK over the Gamma-Gamma fading with zero and nonzero boresight pointing errors.

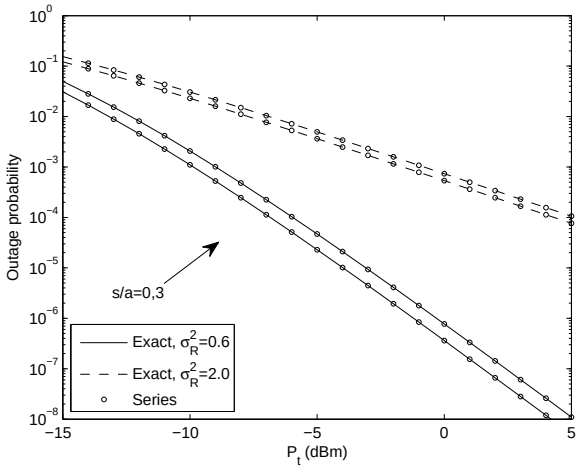

Fig. 6. Outage probability of an FSO system over the Gamma-Gamma fading with zero and nonzero boresight pointing errors.

TABLE I
SYSTEM SETTINGS

Parameter	Value
Receiver Diameter ($2a$)	20 cm
Noise standard deviation (σ_n)	$\sigma_n = 10^{-7}$ A/Hz
Link distance	1 km
Transmit Divergence at $1/e$	1 mrad
Corresponding beam radius (ω_z)	≈ 100 cm
Jitter angle	0.1 mrad
Corresponding jitter standard deviation (σ_s)	≈ 10 cm

boresight error, we use two different values of normalized boresight displacement $s/a = 0, 3$.

In weak turbulence regime, we study the BER of an FSO link over the lognormal fading channel with nonzero boresight pointing errors. We calculate the exact BER from (16), the approximate BER from (24), and the asymptotic BER from (33). The BER curves are plotted in Fig. 1 against the transmitted optical power P_t. From Fig. 1, we can see how the boresight displacement s affects the BER performance of the system. We can infer from the result that for a Gaussian beam

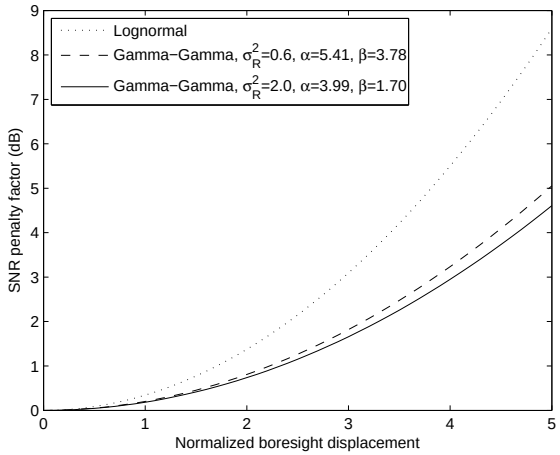

Fig. 7. The SNR penalty factor induced by boresight error in different turbulence conditions.

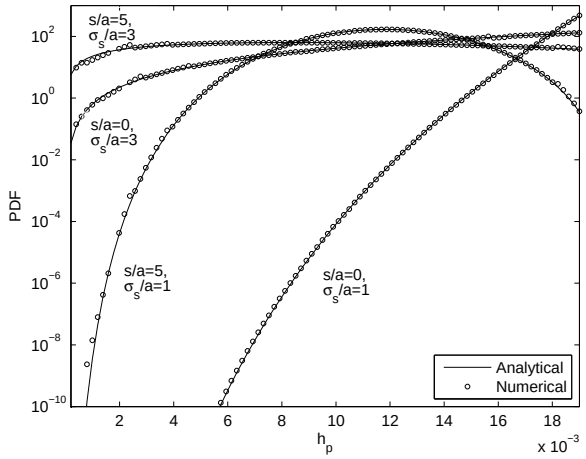

Fig. 8. Comparison of the analytical PDF in (5) and the exact PDF of h_p under various system settings ($w_z/a = 10$).

the energy collected at receiver aperture decreases with increasing boresight errors, and therefore the BER performance deteriorates with a large boresight displacement. However, if we assume a tophat beam profile, the boresight would not affect the collected power at the receiver as long as the boresight displacement s is smaller than the difference of distance between the beamwidth at receiver and the receiver aperture. From the asymptotic BER curves in Fig. 2 and Fig. 3, we find that the diversity order is determined by the equivalent beamwidth as well as the jitter variance. A similar finding is reported in [15] for a MIMO FSO system with zero boresight. With larger beamwidth or smaller jitter variance, the diversity order of the system becomes larger. The outage probability of an FSO system with code rate $R_0 = 0.5$ (bits per channel use) over the composite lognormal fading channel is presented in Fig. 4, where we use (43) to calculate outage probability. It can be seen that the outage probability of the system worsens with increasing boresight errors.

In medium to strong turbulence regimes, we study the BER of an FSO link over the Gamma-Gamma fading channel with nonzero boresight pointing errors. We calculate the exact BER from (15), the approximate BER from (27) (with $J = \lfloor \gamma^2 - \alpha \rfloor$), and the asymptotic BER from (36). The BER curves are plotted in Fig. 5 against the transmitted power P_t. It can be seen that our series solution developed in (27) can accurately approximate the exact BER when P_t is beyond a certain threshold (see Appendix F). However, for small values of P_t, the series approximation in (27) can be inaccurate. This is the limitation of the series approach for the Gamma-Gamma channels with pointing errors, and the same limitation can also be seen from Fig. 2 of [16]. As expected, the BER performance worsens when the boresight displacement s becomes larger. Moreover, the boresight error causes a horizontal shift of the BER curve, resulting in an SNR penalty factor for the error rate performance. From the asymptotic curves in Fig. 5 we can find that the boresight displacement does not affect the diversity order of the system. Assuming a code rate of $R_0 = 0.5$ (bits per channel use), we present the exact outage probability obtained from (C.1) and (42), and the approximate outage probability calculated using (44) in Fig. 6, and it can be seen that the approximate outage probability is accurate. (The threshold of P_t for accurate outage probability approximation is shown in Appendix F.) In Fig. 7, we plot the SNR penalty factor versus the normalized boresight displacement s in both composite lognormal and composite Gamma-Gamma cases. The result indicates that the boresight displacement has larger penalty factor on SNR when the turbulence is weaker.

V. Conclusions

A nonzero boresight pointing error model was investigated for a Gaussian laser beam propagating through atmospheric channels by taking into account the beamwidth, detector aperture, and jitter variance. Our derivation is based on the assumption that the boresight component of pointing error effects is not negligible. A closed-form PDF was derived for the nonzero boresight pointing error model. We derived closed-form composite PDF for the lognormal fading. We also derived an approximate PDF for the Gamma-Gamma fading under the condition $\gamma^2 > \alpha$, which is suitable for terrestrial FSO systems impaired by building sway. Highly accurate convergent series BER expression was obtained for the lognormal fading. The series approximation of BER over the Gamma-Gamma channels can lead to inaccurate estimation if the transmitter power is not sufficiently large. Based on the asymptotic analysis, we observed that the boresight error causes an SNR penalty factor on error rate performance at high SNR. By examining the asymptotic BER curves, we found that the diversity order of the FSO system over the composite lognormal fading channel is solely determined by the pointing error parameter γ^2 and the boresight component does not affect the diversity order. While in the composite Gamma-Gamma fading channel, the diversity order is determined by either the Gamma-Gamma fading effect or the pointing error effect.

APPENDIX A
ANALYTICAL AND NUMERICAL RESULTS OF $f_{h_p}(h_p)$

When a Gaussian beam propagates through distance z from the transmitter to a circular detector with aperture radius a, the fraction of the collected power at receiver is [8]

$$h_p(r;z) = G(r) \triangleq \int_{-a}^{a}\int_{-\sqrt{a^2-x'^2}}^{\sqrt{a^2-x'^2}} \frac{2}{\pi w_z^2} \exp\left(-2\frac{(x'-r)^2+y'^2}{w_z^2}\right) dy'dx' \tag{A.1}$$

where r is the instantaneous radial displacement between the beam centroid and the detector center. We use the approximation given in (2) to derive the analytical PDF of h_p in (5), and the approximation in (2) has normalized mean-squared error less than 10^{-3} when $w_z/a > 6$. Using (A.1), we obtain the exact PDF of h_p as

$$f_{h_p}(h_p) = f_r(G^{-1}(h_p)) \cdot \frac{dG^{-1}(h_p)}{dh_p}. \tag{A.2}$$

Since there is no explicit expression of $G^{-1}(h_p)$, we calculate it numerically. In Fig. 8, we compare the analytical PDF of h_p in (5) as well as the exact PDF of h_p without using (2) under various system settings. It is shown that our analytical model in (5) is accurate even with large boresight ($s/a = 5$) and large jitter ($\sigma_s/a = 3$).

APPENDIX B
DERIVATION OF THE MOMENTS OF h_p

The moments of the generalized pointing error h_p are given by

$$E\left[h_p^n\right] = \int_0^{A_0} h_p^n f_{h_p}(h_p) dh_p. \tag{B.1}$$

Substituting (5) into (B.1), we obtain

$$E\left[h_p^n\right] = \int_0^{A_0} \frac{\gamma^2 \exp\left(-\frac{s^2}{2\sigma_s^2}\right)}{A_0^{\gamma^2}} h_p^{n+\gamma^2-1} I_0\left(\frac{s\nu}{\sigma_s^2}\right) dh_p \tag{B.2}$$

where $\nu = \sqrt{\frac{-\omega_{z_{eq}}^2 \ln\frac{h_p}{A_0}}{2}}$. Using a series representation of $I_0(\cdot)$ [35, Eq.(8.445)], we have

$$E\left[h_p^n\right] = \frac{\gamma^2 \exp\left(-\frac{s^2}{2\sigma_s^2}\right)}{A_0^{\gamma^2}} \int_0^{A_0} h_p^{n+\gamma^2-1} \sum_{m=0}^{\infty} \frac{1}{(m!)^2}\left(\frac{s\nu}{2\sigma_s^2}\right)^{2m} dh_p. \tag{B.3}$$

Since each term of the series is non-negative and the infinite series uniformly converges to $I_0\left(\frac{s\nu}{\sigma_s^2}\right)$, we can swap the integral and infinite summation and write (B.3) as

$$\begin{aligned} E\left[h_p^n\right] &= \frac{\gamma^2 \exp\left(-\frac{s^2}{2\sigma_s^2}\right)}{A_0^{\gamma^2}} \times \sum_{m=0}^{\infty} \frac{1}{(m!)^2} \int_0^{A_0} h_p^{n+\gamma^2-1} \left(\frac{s^2}{4\sigma_s^4} \cdot \frac{-\omega_{z_{eq}}^2 \ln\frac{h_p}{A_0}}{2}\right)^m dh_p \\ &= \frac{\gamma^2 \exp\left(-\frac{s^2}{2\sigma_s^2}\right)}{A_0^{\gamma^2}} \times \sum_{m=0}^{\infty} \left[\frac{\left(\frac{-\omega_{z_{eq}}^2 s^2}{8\sigma_s^4}\right)^m}{(m!)^2} A_0^{n+\gamma^2} \int_0^1 x^{n+\gamma^2-1} (\ln x)^m dx\right]. \end{aligned} \tag{B.4}$$

Applying an integral identity [35, Eq.(4.294.10)] to (B.4), we have

$$\begin{aligned} E\left[h_p^n\right] &= \gamma^2 \exp\left(-\frac{s^2}{2\sigma_s^2}\right) A_0^n \sum_{m=0}^{\infty} \left[\frac{\left(\frac{\gamma^2 s^2}{2\sigma_s^2(n+\gamma^2)}\right)^m}{m!} \frac{1}{(n+\gamma^2)}\right] \\ &= \frac{A_0^n \gamma^2}{n+\gamma^2} \exp\left(-\frac{n s^2}{(n+\gamma^2)2\sigma_s^2}\right). \end{aligned} \tag{B.5}$$

APPENDIX C
GAMMA-GAMMA COMPOSITE PDF

1) Composite PDF Approximation: We substitute (8) into (9) and write the composite PDF of the Gamma-Gamma fading with nonzero boresight pointing error as (C.1) at the top of next page. Applying a change of variable rule $x = \sqrt{-\frac{w_{z_{eq}}^2}{2} \ln\left(\frac{h}{h_a A_0 h_l}\right)}$, eq. (C.1) can be expressed as (C.2), where $W(h) = h^{\frac{\alpha+\beta}{2}-1} K_{\alpha-\beta}\left(2\sqrt{\frac{\alpha\beta h}{A_0 h_l}} \exp\left(\frac{x^2}{w_{z_{eq}}^2}\right)\right)$. Using a series expansion of the modified Bessel function of the second kind [34, eq. (03.04.06.0002.01)]

$$K_v(x) = \frac{\pi}{2\sin(\pi v)} \sum_{p=0}^{\infty} \left[\frac{(x/2)^{2p-v}}{\Gamma(p-v+1)p!} - \frac{(x/2)^{2p+v}}{\Gamma(p+v+1)p!}\right] \tag{C.3}$$

where it requires $v \notin \mathbb{Z}$ and $|x| < \infty$, we can express $W(h)$ as

$$\begin{aligned} W(h) = \frac{\pi}{2\sin(\pi(\alpha-\beta))} \sum_{j=0}^{\infty} \Bigg(&\frac{\left(\frac{\alpha\beta}{A_0 h_l} \exp\left(\frac{2x^2}{w_{z_{eq}}^2}\right)\right)^{j-\frac{\alpha-\beta}{2}}}{\Gamma(j-(\alpha-\beta)+1)j!} h^{j+\beta-1} \\ &- \frac{\left(\frac{\alpha\beta}{A_0 h_l} \exp\left(\frac{2x^2}{w_{z_{eq}}^2}\right)\right)^{j+\frac{\alpha-\beta}{2}}}{\Gamma(j+(\alpha-\beta)+1)j!} h^{j+\alpha-1} \Bigg). \end{aligned} \tag{C.4}$$

$$f_{GG}(h) = \frac{2\gamma^2 \exp(-s^2/2\sigma_s^2)(\alpha\beta)^{(\alpha+\beta)/2}}{(A_0 h_l)^{\gamma^2}\Gamma(\alpha)\Gamma(\beta)} h^{\gamma^2-1} \times \int_{h/(A_0 h_l)}^{\infty} h_a^{\frac{\alpha+\beta}{2}-\gamma^2-1} I_0\left(\frac{s}{\sigma_s^2}\sqrt{-\frac{w_{z_{eq}}^2}{2}\ln\left(\frac{h}{h_a A_0 h_l}\right)}\right) K_{\alpha-\beta}(2\sqrt{\alpha\beta h_a}) dh_a \tag{C.1}$$

$$f_{GG}(h) = \frac{8\gamma^2 \exp(-s^2/2\sigma_s^2)(\alpha\beta)^{(\alpha+\beta)/2}}{(A_0 h_l)^{\frac{\alpha+\beta}{2}}\Gamma(\alpha)\Gamma(\beta) w_{z_{eq}}^2} \int_0^{\infty} x \exp\left(\frac{2x^2}{w_{z_{eq}}^2}\left(\frac{\alpha+\beta}{2}-\gamma^2\right)\right) I_0\left(\frac{s}{\sigma_s^2}x\right) W(h) dx \tag{C.2}$$

$$\begin{aligned} f_{GG}(h) = & \\ & \frac{4\pi\gamma^2 \exp(-s^2/2\sigma_s^2)(\alpha\beta)^{(\alpha+\beta)/2}}{(A_0 h_l)^{(\alpha+\beta)/2}\Gamma(\alpha)\Gamma(\beta)\sin((\alpha-\beta)\pi) w_{z_{eq}}^2} h^{(\alpha+\beta)/2-1} \\ & \times \sum_{j=0}^{\infty}\left(\frac{1}{\Gamma(j-(\alpha-\beta)+1)j!}\left(\frac{\alpha\beta h}{A_0 h_l}\right)^{j-(\alpha-\beta)/2}\int_0^{\infty} x\exp\left(\frac{2x^2}{w_{z_{eq}}^2}(\beta-\gamma^2+j)\right) I_0\left(\frac{s}{\sigma_s^2}x\right) dx\right. \\ & \left. -\frac{1}{\Gamma(j+(\alpha-\beta)+1)j!}\left(\frac{\alpha\beta h}{A_0 h_l}\right)^{j+(\alpha-\beta)/2}\int_0^{\infty} x\exp\left(\frac{2x^2}{w_{z_{eq}}^2}(\alpha-\gamma^2+j)\right) I_0\left(\frac{s}{\sigma_s^2}x\right) dx\right) \end{aligned} \tag{C.5}$$

Substituting (C.4) into (C.2), and after some manipulation, we have (C.5).

In the following derivation, we use an integral identity [35, eq. (6.643.2)]

$$\begin{aligned} & \int_0^{\infty} x^{u-\frac{1}{2}} e^{-\alpha x} I_{2v}(2\beta\sqrt{x}) dx \\ & = \frac{\Gamma\left(u+v+\frac{1}{2}\right)}{\Gamma(2v+1)}\beta^{-1}\exp\left(\frac{\beta^2}{2\alpha}\right)\alpha^{-u} M_{-u,v}\left(\frac{\beta^2}{\alpha}\right) \end{aligned} \tag{C.6}$$

where $M_{u,v}(\cdot)$ is the Whittaker function. Hence, by using another the identity [34, eq. (07.44.03.0041.01)]

$$M_{\frac{m-1}{2},\frac{m}{2}}(z) = \exp\left(-\frac{z}{2}\right) z^{\frac{1-m}{2}} m!\left(\exp(z) - \sum_{k=0}^{m-1}\frac{z^k}{k!}\right), \quad m \geq 0 \tag{C.7}$$

we can represent (C.5) as (12). In our derivation, the integral identity (C.3) requires that $(\alpha-\beta) \notin \mathbb{Z}$, and the integral identity (C.6) requires that the summation index j in (C.5) must be lower than or equal to $J = \lfloor \gamma^2 - \alpha \rfloor$, where $\lfloor x \rfloor$ denotes the largest integer not greater than x. Such truncation method is also used in [16] to estimate the BER of systems over the Gamma-Gamma channels with Hoyt distributed pointing error. Due to the truncation of the infinite series and the constraint on the number of terms $j \leq \lfloor \gamma^2 - \alpha \rfloor$, our series PDF in (12) may not converge to the exact PDF for weak turbulence. However, beyond certain threshold of transmit power P_t (shown in Appendix F), the approximate BER is accurate since the PDF $f_{GG}(h)$ near the origin can be accurately described by (12).

2) PDF Near the Origin: To obtain the power series expansion of the Gamma-Gamma composite PDF near the origin, we can express $W(h)$ as

$$\lim_{h\to 0} W(h) = \frac{\pi\left(\frac{\alpha\beta}{A_0 h_l}\exp\left(\frac{2x^2}{w_{z_{eq}}^2}\right)\right)^{-\frac{\alpha-\beta}{2}}}{2\sin(\pi(\alpha-\beta))\Gamma(-(\alpha-\beta)+1)} h^{\beta-1} + g_{\beta-1}(h). \tag{C.8}$$

From (C.8) and (C.2), we can derive the PDF near the origin as

$$\lim_{h\to 0} f_{GG}(h) = \frac{\gamma^2\pi\left(\frac{\alpha\beta}{A_0 h_l}\right)^{\beta}\exp\left(-\frac{s^2}{2\sigma_s^2}-\frac{s^2\gamma^2/\sigma_s^2}{2\beta-2\gamma^2}\right)\sin^{-1}((\alpha-\beta)\pi)}{\Gamma(\alpha)\Gamma(\beta)\Gamma(-(\alpha-\beta)+1)|-(\beta-\gamma^2)|} h^{\beta-1} + g_{\beta-1}(h). \tag{C.9}$$

APPENDIX D
BOUND ON APPROXIMATION ERROR

By applying an upper bound $\mathrm{erfc}(x) < \exp(-x^2)$ to (19), we can upper bound R_B as

$$\begin{aligned} R_B < & \\ & \frac{\gamma^2 u_c}{4}\exp\left(u_a - \gamma^2 u_b\right) \\ & \times \int_B^{\infty}\exp\left(\gamma^2 u_c x - x^2 - \frac{P_t^2}{2\sigma_n^2}A_0^2 h_l^2\exp(u_c x - b)\right) dx \\ & < \frac{\gamma^2 u_c}{4}\exp\left(u_a - \gamma^2 u_b\right)\int_B^{\infty}\exp\left(\gamma^2 u_c x - x^2\right) dx. \end{aligned} \tag{D.1}$$

Using an integral identity [35, Eq.(2.33.1)]

$$\int \exp(-(ax^2+2bx+c))dx = \frac{1}{2}\sqrt{\frac{\pi}{a}}\exp\left(\frac{b^2-ac}{a}\right)\mathrm{erf}\left(\sqrt{a}x+\frac{b}{\sqrt{a}}\right) \tag{D.2}$$

we derive the upper bound for R_B as

$$R_B < \frac{\sqrt{\pi}\gamma^2 u_c}{8}\exp\left(u_a-\gamma^2\left(u_b-\frac{\gamma^2u_c^2}{4}\right)\right)\mathrm{erfc}\left(B-\frac{\gamma^2u_c}{2}\right). \tag{D.3}$$

For different R_B, the required values of B, which are calculated by (D.3), are shown in Table III, where we set $w_z/a = 10, s/a = 1.0, \sigma_s/a = 1.0$. It is found that the approximation error R_B decreases rapidly with increasing B, and therefore we can adjust the value of B to make R_B arbitrarily small.

APPENDIX E
PROOF OF CONVERGENCE OF SERIES

The series in (24) contains the expression

$$P_S = \frac{2}{\sqrt{\pi}}\sum_{j=0}^{\infty}\frac{(-1)^j}{j!(2j+1)}\left(\frac{P_tA_0h_l}{\sqrt{2}\sigma_n}\right)^{2j+1}\frac{\exp(-u_b(2j+1))}{(2j+1+\gamma^2)u_c}S_j. \tag{E.1}$$

We now use the ratio test to assess the convergence of this series. The absolute ratio between two consecutive terms is

$$\left|\frac{a_{j+1}}{a_j}\right| = \frac{(2j+1)\left(\frac{P_tA_0h_l}{\sqrt{2}\sigma_n}\right)^2\exp(-2u_b)(2j+1+\gamma^2)}{(j+1)(2j+3)(2j+3+\gamma^2)}\cdot\frac{S_{j+1}}{S_j}. \tag{E.2}$$

By applying the bounds of the $\mathrm{erfc}(\cdot)$ function [41]

$$\frac{1}{\sqrt{\pi}x}\left(1-\frac{1}{2x^2}\right)\exp(-x^2) < \mathrm{erfc}(x) < \frac{1}{\sqrt{\pi}x}\exp(-x^2) \tag{E.3}$$

to S_{j+1} (upper bound) and S_j (lower bound), we have

$$\frac{S_{j+1}}{S_j} < \frac{\frac{1}{B}+\frac{1}{(\gamma^2+2j+3)\frac{u_c}{2}-B}\exp(2Bu_c)}{\frac{1}{B}\left(1-\frac{1}{2B^2}\right)+\frac{1}{(\gamma^2+2j+1)\frac{u_c}{2}-B}\left(1-\frac{1}{2((\gamma^2+2j+1)\frac{u_c}{2}-B)^2}\right)}. \tag{E.4}$$

Applying the limit operation to both sides of (E.4) and noting that S_j and S_{j+1} are positive, we have

$$0 < \lim_{j\to\infty}\frac{S_{j+1}}{S_j} < \frac{1}{1-\frac{1}{2B^2}}. \tag{E.5}$$

For the rest of the terms in (E.2), we have

$$\lim_{j\to\infty}\frac{(2j+1)\left(\frac{P_tA_0h_l}{\sqrt{2}\sigma_n}\right)^2\exp(-2u_b)(2j+1+\gamma^2)}{(j+1)(2j+3)(2j+3+\gamma^2)} = 0. \tag{E.6}$$

Since limits in (E.5) and (E.6) both exist, we have

$$\lim_{j\to\infty}\left|\frac{a_{j+1}}{a_j}\right| = \lim_{j\to\infty}\frac{(2j+1)\left(\frac{P_tA_0h_l}{\sqrt{2}\sigma_n}\right)^2(2j+1+\gamma^2)}{\exp(2u_b)(j+1)(2j+3)(2k+3+\gamma^2)}\cdot\lim_{j\to\infty}\frac{S_{j+1}}{S_j} = 0. \tag{E.7}$$

Thus, we have $\lim_{j\to\infty}\left|\frac{a_{j+1}}{a_j}\right| = 0$. We conclude that the series P_S in (24) is convergent.

APPENDIX F
APPROXIMATION ERROR

After the numerical evaluation of the approximation error in (27) under different system parameters, we find our series solutions in (27) and (44) may not approach to the exact results when P_t is small. This is a limitation of the series approach. In Table IV, we show the minimum required P_t that can guarantee the relative error $\frac{\varepsilon(P_e)}{P_e} < 10^{-6}$ and $\frac{\varepsilon(P_{out})}{P_{out}} < 10^{-6}$ for three representative turbulence conditions. From Table IV, we observe that the minimum required P_t becomes larger with increasing boresight or jitter.

REFERENCES

[1] S. Kartalopoulos. *Free Space Optical Networks for Ultra-Broad Band Services*. New York: Wiley, 2011.

[2] I. I. Kim, R. Stieger, J. A. Koontz, C. Moursund, M. Barclay, P. Adhikari, J. Schuster, E. Korevaar, R. Ruigrok, and C. DeCusatis, "Wireless optical transmission of fast ethernet, FDDI, ATM, and ESCON protocol data using the TerraLink laser communication system," *Optical Engineering*, vol. 37, pp. 3143-3155, Dec. 1998 .

[3] D. K. Borah and D. G. Voelz, "Estimation of laser beam pointing parameters in the presence of atmospheric turbulence," *Applied Optics*, vol. 46, pp. 6010-6018, Aug. 2007.

[4] D. K. Borah and D. G. Voelz, "Pointing error effects on free-space optical communication links in the presence of atmospheric turbulence," *IEEE/OSA J. Lightwave Technol.*, vol. 27, pp. 3965-3973, Sept. 2009.

[5] C. C. Chen and C. Gardner, "Impact of random pointing and tracking errors on the design of coherent and incoherent optical intersatellite communication links," *IEEE Trans. Commun.*, vol. 37, pp. 252-260, Mar. 1989.

[6] S. Arnon, "Optimization of urban optical wireless communication systems," *IEEE Trans. Wireless. Commun.*, vol. 2, pp. 626-629, July 2003.

[7] D. K. Borah, D. Voelz, and S. Basu, "Maximum-likelihood estimation of a laser system pointing parameters by use of return photon counts," *Appl. Opt.*, vol. 45, pp. 2504-2509, Apr. 2006.

[8] A. Farid and S. Hranilovic, "Outage capacity optimization for free-space optical links with pointing errors," *IEEE/OSA J. Lightwave Technol.*, vol. 25, pp. 1702-1710, July 2007.

[9] S. Arnon, "Effects of atmospheric turbulence and building sway on optical wireless-communication systems," *Opt. Lett.*, vol. 28, pp. 129-131, Jan. 2003.

[10] H. Sandalidis, T. Tsiftsis, G. Karagiannidis, and M. Uysal. "BER performance of FSO links over strong atmospheric turbulence channels with pointing errors," *IEEE Commun. Lett.*, vol. 12, pp. 44-46, Jan. 2008.

[11] H. Sandalidis, T. Tsiftsis, and G. Karagiannidis, "Optical wireless communications with heterodyne detection over turbulence channels with pointing errors," *IEEE/OSA J. Lightwave Technol.*, vol. 27, pp. 4440-4445, Oct. 2009.

[12] X. Liu, "Free-space optics optimization models for building sway and atmospheric interference using variable wavelength," *IEEE Trans. Commun.*, vol. 57, pp. 492-498, Feb. 2009.

[13] W. Gappmair, S. Hranilovic, and E. Leitgeb, "Performance of PPM on terrestrial FSO links with turbulence and pointing errors," *IEEE Commun. Lett.*, vol. 14, pp. 468-470, May 2010.

TABLE III
VALUES OF B FOR DIFFERENT R_B VALUES

Parameters	$R_B = 10^{-6}$	$R_B = 10^{-8}$	$R_B = 10^{-10}$
$\sigma_R^2 = 0.05$	7.60	8.18	8.69
$\sigma_R^2 = 0.1$	9.28	9.86	10.36
$\sigma_R^2 = 0.2$	11.65	12.22	12.73

TABLE IV
MINIMUM REQUIRED $P_t(\mathrm{dBm})$ FOR $\frac{\varepsilon(P_e)}{P_e} < 10^{-6}$ AND $\frac{\varepsilon(P_{out})}{P_{out}} < 10^{-6}$

Parameters	$s/a = 1.0, \sigma_s/a = 1.0$	$s/a = 1.0, \sigma_s/a = 1.5$	$s/a = 2.0, \sigma_s/a = 1.5$
$\sigma_R^2 = 0.6; \alpha = 5.41, \beta = 3.78$	-14, -18	-1, -5	9, 5
$\sigma_R^2 = 2.0; \alpha = 3.99, \beta = 1.70$	-19, -23	-8, -12	6, 2
$\sigma_R^2 = 4.0; \alpha = 4.34, \beta = 1.31$	-19, -23	-13, -17	-9, -12

[14] A. García-Zambrana, B. Castillo-Vázquez, and C. Castillo-Vázquez, "Asymptotic error-rate analysis of FSO links using transmit laser selection over gamma-gamma atmospheric turbulence channels with pointing errors," *Opt. Express*, vol. 20, pp. 2096-2109, Jan. 2012.

[15] A. Farid and S. Hranilovic, "Diversity gain and outage probability for MIMO free-space optical links with misalignment," *IEEE Trans. Commun.*, vol. 60, pp. 479-487, Feb. 2012.

[16] W. Gappmair, S. Hranilovic, and E. Leitgeb, "OOK performance for terrestrial FSO links in turbulent atmosphere with pointing errors modeled by Hoyt distributions," *IEEE Commun. Lett.*, vol. 15, pp. 875-877, Aug. 2011.

[17] S. Bloom, E. Korevaar, J. Schuster, and H. Willebrand, "Understanding the performance of free-space optics," *Journal of Optical Networking*, vol. 2, pp. 178-200, June 2003.

[18] D. K. Borah, D. G. Voelz, and S. Basu, "Maximum-likelihood estimation of a laser system pointing parameters by use of return photon counts," *Applied Optics*, vol. 45, pp. 2504-2509, Apr. 2003.

[19] J. Recolons, L. C. Andrews, and R. L. Phillips, "Analysis of beam wander effects for a horizontal-path propagating Gaussian-beam wave: focused beam case," *Optical Engineering*, vol. 46, pp. 086002-086002, Aug. 2007.

[20] I. Buske and W. Riede, "Atmospheric tip/tilt compensation for laser beam tracking with amateur telescopes," *Proc. SPIE. 7483*, pp. 74830S-74830S, Sept. 2009.

[21] G. Lukesh, S. Chandler, and D. G. Voelz, "Estimation of laser system pointing performance by use of statistics of return photons," *Applied Optics*, vol. 39, pp. 1359-1371, Mar. 2000.

[22] V. S. R. Gudimetla and J. F. Riker, "Moment-matching method for extracting beam jitter and boresight in experiments with satellites of small physical cross section," *Applied Optics*, vol. 46, pp. 5608-5616, Aug. 2007.

[23] Z. Zhao and R. Liao, "Fading probability density function of free-space optical communication channels with pointing error," *Proc. SPIE 8038*, pp. 803-805, May 2011.

[24] S. M. Navidpour, M. Uysal, and M. Kavehrad, "BER performance of free-space optical transmission with spatial diversity," *IEEE Trans. Wireless Commun.*, vol. 6, pp. 2813-2819, Aug. 2007.

[25] T. Tsiftsis, H. Sandalidis, G. Karagiannidis, and M. Uysal, "Optical wireless links with spatial diversity over strong atmospheric turbulence channels," *IEEE Trans. Wireless Commun.*, vol. 8, pp. 951-957, Feb. 2009.

[26] P. Beckmann and A. Spizzichino, *The Scattering of Electromagnetic Waves from Rough Surfaces*. MA: Artech House, 1987.

[27] J. H. Churnside and S. F. Clifford, "Log-normal Rician probability density function of optical scintillations in the turbulent atmosphere," *J. Opt. Soc. Am. A*, vol. 4, pp. 1923-1930, Oct. 1987.

[28] F. Yang and J. Cheng, "Coherent free-space optical communications in lognormal-Rician turbulence," *IEEE Commun. Lett.*, vol.16, pp.1872-1875, Nov. 2012.

[29] M. K. Simon and M. S. Alouini, *Digital Communication over Fading Channels*. New York: Wiley, 2005.

[30] S. Karp, *Optical Channels: Fibers, Clouds, Water, and the Atmosphere*. Applications of Communications Theory, New York: Plenum Press, 1988.

[31] M. A. Al-Habash, L. C. Andrews, and R. L. Phillips, "Mathematical model for the irradiance probability density function of a laser beam propagating through turbulent media," *Optical Engineering*, vol. 40, pp. 1554-1562, Aug. 2001.

[32] N. Perlot, *Characterization of Signal Fluctuations in Optical Communications with Intensity Modulation and Direct Detection Through the Turbulent Atmospheric Channel*. Berichte aus der Kommunikationstechnik, Shaker Verlag GmbH, 2005.

[33] E. Bayaki, R. Schober, and R. K. Mallik, "Performance analysis of MIMO free-space optical systems in gamma-gamma fading," *IEEE Trans. Commun.*, vol. 57, pp.3415-3424, Nov. 2009.

[34] Wolfram, "The wolfram functions site: http://functions.wolfram.com/," 2001.

[35] I. S. Gradshteyn and I. M. Ryzhik, *Table of Integrals, Series, and Products, 7th ed*. New York: Academic Press, 2007.

[36] Z. Wang and G. B. Giannakis, "A simple and general parameterization quantifying performance in fading channels," *IEEE Trans. Commun.*, vol. 51, pp. 1389-1398, Aug. 2003.

[37] X. Song, F. Yang, and J. Cheng, "Subcarrier intensity modulated optical wireless communications in atmospheric turbulence with pointing errors," *IEEE/OSA J. Opt. Netw.*, vol. 5, pp. 349-358, Apr. 2013.

[38] L. Zheng and D. N. C. Tse, "Diversity and multiplexing: a fundamental tradeoff in multiple-antenna channels," *IEEE Trans. Inform. Theory*, vol. 49, pp. 1073-1096, May 2003.

[39] I. I. Kim, B. McArthur, and E. J. Korevaar, "Comparison of laser beam propagation at 785 nm and 1550 nm in fog and haze for optical wireless communications," *Proc. SPIE 4214*, pp. 26-37, Feb. 2001.

[40] E. J. Korevaar, I. I. Kim, and B. McArthur, "Atmospheric propagation characteristics of highest importance to commercial free space optics," *Proc. SPIE 4976*, pp. 1-12, Apr. 2003.

[41] J. M. Wozencraft and I. M. Jacobs, *Principles of Communication Engineering*. Waveland Press, 1990.